Green Chemistry

Accepted Manuscript

ROYAL SOCIETY OF CHEMISTRY

www.rsc.org/greenchem

Journal Name

ARTICLE

Removal and safe reuse of highly toxic allyl alcohol by highly selective photo-sensitive metal-organic framework

Received 00th January 20xx,
Accepted 00th January 20xx

DOI: 10.1039/x0xx00000x

www.rsc.org/

Feng Luo,[1]* Le Le Gong,[1] Xue Feng Feng,[1] Xian Feng Yi,[2] and An Min Zheng*[2]

Herein, we report a facile and green approach to remove, convert and even release highly toxic allyl alcohol inside MOF. The MOF used here, namely **ECIT-20**, barely adsorbs allyl alcohol under ambient condition, whereas sharp increase up to 90 mg/g (1.03mol/mol) under UV (297 nm) irradiation is observed, giving an ultra-big photo-switching behavior of more than 19 times. Thermogravimetry, infrared spectroscopy, and ^{1}H MAS plus ^{13}C CPMAS solid-state NMR spectrum showed that the host-guest photochemical [2+2] reaction and next formation of asymmetric cyclobutanes is responsible for this unique photo-switching behavior towards allyl alcohol. The final conversion capability by means of **ECIT-20** from allyl alcohol to asymmetric cyclobutanes is estimated to be 0.5mol/mol, which agrees well with both the structure feature and the results from the density functional theory (DFT) calculations. Moreover, the reuse of this MOF material is also facile and even after four cycles, excellent photo-switching performance towards allyl alcohol could be well maintained. This indicates highly promising material of **ECIT-20** for green removal and safe reuse of highly toxic allyl alcohol.

Introduction

Allyl alcohol is a very important raw material and widely used as chemical intermediates to synthesize glycerin, medicine, pesticides, spices and cosmetics.[1-3] Like that of H_2, CH_4, and C_2H_2 molecules,[4] allyl alcohol is inflammable and explosive cargo when its content in air is more than 2.5%. This nature makes the safe storage and transportation become very challenging. Besides, allyl alcohol is also highly toxic. Accordingly, the utilization of allyl alcohol inevitably causes a series of environmental problems and even directly affects the safety of human life. It is thus very important and mandatory for us to probe not only high-performance but also green and safe removal and storage approach to minimize their negative impact.

Metal-organic frameworks (MOFs) are now receiving explosive interests and have been attested to perform remarkable potential in loading various cargos such as gas (CO_2, H_2, CH_4, C_2H_2*et al*)[5-17] and metal ions (Hg^{2+}, UO^{2+} *et al*).[18-23] This high-performance capture is mainly due to the strong host-guest interactions derived from coordination-unsaturated metal sites, free standing functional groups, or exactly matching aperture.[24-26] Note that except for the above excellent physical adsorption performance, in some cases exceptional adsorption and next conversion, which is accompanied by chemical reaction, was observed.[27-29] However, to remove and reclaim highly toxic cargos such asallyl alcohol, 100 percent adsorption technique based on MOF materials is not the best, as first the inherent nature determined that this kind of fixing is not stable, then we must also face to some crucial problems like that of the reuse of MOF materials and safe release, *et al*. In this regard, the biggest challenge at present is seeking out robust MOF materials that could convert highly toxic cargo into a part of their own *via* chemical reaction, and simultaneously, the safe release of highly toxic cargo after conversion inside MOFs could be achieved by applying some external stimulus to advance the occurrence of reversible chemical reaction.

Taking the above into account, we here designed and synthesized a potentially photo-sensitive MOF, $[Zn(L)(bpe)]_n\cdot(H_2O)_3(DMF)_{1.5}$($H_2L$= 2,2'-dinitro-[1,1'-biphenyl]-4,4'-dicarboxylic acid, bpe= trans-1,2-bis(4- pyridyl)ethane, **ECIT-20**). Unlike that of documented photo-switching MOFs characterized by *trans*-to-*cis* transformation of azobenzene unit or *open-ring*-to-*close-ring* transformation of diarylethene unit,[30-39] the present MOF undergoes uncommon type in this way of photochemical [2+2] reaction between MOF skeleton and allyl alcohol. **ECIT-20** barely adsorbs allyl alcohol under ambient condition, whereas sharp increase up to 90 mg/g (1.03mol/mol) under UV (297 nm) irradiation is observed, giving an ultra-big photo-switching behavior of more than 19 times. And the resulted asymmetric cyclobutanes show thermo-dependent reversible cleavage, which facilitates to rerelease allyl alcohol. Notably, such cycle from photochemical [2+2]cycloaddition (fixing allyl alcohol) to reversible cleavage of cyclobutane (rereleasing allyl alcohol) could be cycled at least four times. Our findings contribute to provide a not only high-performance but also green and safe pathway for removal and reuse of highly toxic allyl alcohol.

Experimental Section

Synthesis.

ECIT-20. A DMF solution (6 mL) of $Zn(NO_3)_2\cdot 6H_2O$, H_2L, and bpe in a ratio of 1:1:1 was sealed in a Teflon reactor, and heated at 110˚C for 3 days, and then cooled to room temperature at 3˚C/h. Subsequently, pure block crystals were yielded and dried naturally in air for three days to obtain product with 90% yield based on Zn. Element analysis: calc. C/49.41, N/10.38, H/4.42; exp. C/49.23, N/10.31, H/4.36.

[1]School of Biology, Chemistry and Material Science, East China University of Technology, Nanchang, Jiangxi 344000, China, ecitluofeng@163.com
[2]State Key Laboratory of Magnetic Resonance and Atomic and Molecular Physics, Wuhan Institute of Physics and Mathematics, The Chinese Academy of Sciences, Wuhan 430071, China, zhenganm@wipm.ac.cn
Electronic Supplementary Information (ESI) available: additional Figures. See DOI: 10.1039/x0xx00000x

ECIT-20@1.2DMF. The as-synthesized samples of **ECIT-20** were immerged in CH_3OH for three days. During this, CH_3OH was refreshed three times a day. Then they were degassed in Belsorp-max under vacuum at 200°C for 24h to obtain products. Element analysis: calc. C/53.42, N/10.94, H/3.69; exp. C/53.49, N/10.89, H/3.72.

ECIT-21@1.2DMF. Samples of **ECIT-20@1.2DMF** about 100 mg is used to carried out CH_2=$CHCH_2OH$ adsorption experiment at 298 K. During this, 297 nm UV was irradiated onto the sample tube all through. The samples of **ECIT-21@1.2DMF** were obtained after one circle of adsorption and desorption of CH_2=$CHCH_2OH$. Element analysis: calc. C/53.78, N/10.48, H/3.97; exp. C/53.72, N/10.41, H/3.92.

Materials and General Methods. Reagents and solvents were commercially available and were used without further purification. Thermogravimetric analysis (TGA) was performed by a TGA Q500 thermal analysis system. All TGA experiments were performed under a N_2 atmosphere from 40-800°C at a rate of 5°C /min. Data were analyzed using the TA Universal Analysis software package. X-ray powder diffraction were collected by a Bruker AXS D8 Discover powder diffractometer at 40 kV, 40 mA for Cu Kα, (λ = 1.5406Å). The simulated powder patterns were calculated by Mercury 1.4. The purity of the bulk products were determined by comparison of the simulated and experimental PXRD patterns. Infrared Spectra (IR) were measured by a Bruker VERTEX 70 spectrometer in the 500-4000 cm^{-1} region. The gas sorption isotherms were collected on a Belsorp-max. The as-synthesized sample (weight of about 100 mg) was degassed in the sample tube and dried for 24 h at 200 °C prior to measurements. Ultrahigh-purity-grade (> 99.999%) N_2, CO, O_2, CO_2, and CH_4 gases, ultra pure water and CH_3OH, C_2H_5OH, CH_2=$CHCH_2OH$ in the GC grade were used in this adsorption measurement. To maintain the experimental temperatures liquid nitrogen (77 K), mixed liquid nitrogen and acetone (195 K), and temperature-programmed water bath (273 and 293 K) were used respectively. And 298 K was controlled by close air-condition system and traced by thermometer.

X-ray Crystallography. Unit cell measurements and intensity data were collected at 113 K on a Bruker-AXS SMART Breeze CCD diffractometer using graphite monochromatedMoKα radiation (λ=0.71073 Å). The data reduction included a correction for Lorentz and polarization effects, with an applied multi-scan absorption correction (SADABS). The crystal structure was solved and refined using the SHELXTL program suite. Direct methods yielded all non-hydrogen atoms, which were refined with anisotropic thermal parameters. All hydrogen atom positions were calculated geometrically and were riding on their respective atoms. CCDCnumber is 1411042 for **ECIT-20**. The data can be obtained free of charge (http://www.ccdc.cam.ac.uk/data_request/cif).

Computational methods. Before the simulation of the powder XRD curves, the crystal structures of **ECIT-20** and **ECIT-21**were optimized by the density functional theory (DFT) calculations. Since the structure of **ECIT-21** could not be determined by single crystal X-ray diffraction, and then the **ECIT-21** crystal structure was constructed from the **ECIT-20** through the heterogeneous [2+2] cycloaddition as discussed in our work. Geometry optimizations were carried out by using DFT theoretical method availed in $Dmol^3$ program.[40] During the optimizations, all of the atoms were relaxed to their equilibrium positions, while the lattice parameters of host structure were fixed to the crystallographic values. A double numerical basis set with polarization functions (DNP) at GGA/PW91 theoretical level was used in all calculations.[41] During the optimizations, the convergence threshold tolerance was set as follows: total energy=2×10^{-5} Ha; maximum force =4×10^{-3} Ha/Å. Based on the optimized structures, the simulated powder XRD curves were obtained by using Mercury 1.4.

Results and Discussion

Crystal Structure. The MOF was synthesized through solvothermal reaction of $Zn(NO_3)_2$, H_2L, and bpe in DMF with a ratio of 1:1:1 at 110°C. The phase purity of the bulk samples were confirmed by element analysis (EA) and powder X-ray diffraction (PXRD). Single X-ray diffraction discloses that **ECIT-20** crystalizes in a monoclinic, $P2_1/c$ space group, and the asymmetric unit contains one crystallography-independent Zn(II) ion, which affords a tetrahedral geometry finished by two oxygen atoms from two L^{2-} ligand and two nitrogen atoms from two bpe ligands (Figure 1a). The L^{2-} ligand that is largely distorted with the dihedral angel of ca. 72° for two phenyl groups, adopts a bi(monodentate) coordination mode. This finally results in overall three-fold interpenetrating **dia** net (Figure 1b, c). However, despite interpenetration, we also observed regular 1D channel along *c* axis with the window of 8.0×12.0 $Å^2$ in **ECIT-20**. We further estimated the solvent-accessible volume by Platon program, giving potential solvent-accessible volume of 3676.7 $Å^3$, equal to 62.8% of the cell volume.[42] Moreover, we analyzed the cross-section of pore configuration and found 1D regular channels along *c* axis but staggered channels along *b* axis (Figure 2), as well as tight stacking in *a* axis direction (Figure 1b).

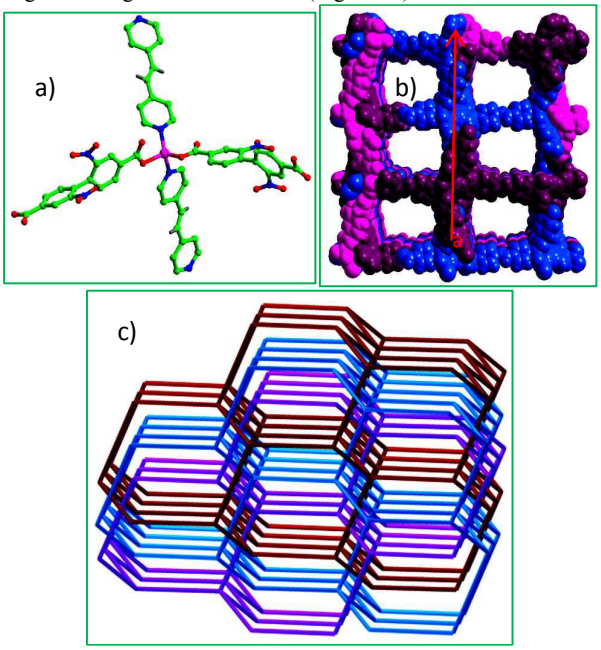

Figure 1. a) View of the coordination surrounding around metal ion; b) spacefill view of the three-fold interpenetrating net of **ECIT-20** (each color presents one identical net); c) schematic description of the three-fold interpenetrating net with **dia** topology matrix.

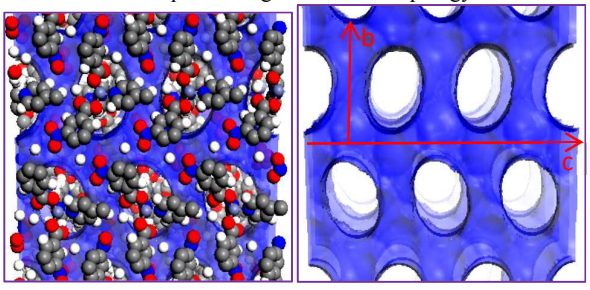

Figure 2. View of the pore configuration in **ECIT-20**: pore plus MOF skeleton/left; pore/right.

Thermostability and Adsorption Properties. To obtain guest-free framework of **ECIT-20**, the as-synthesized samples were degassed and traced by element analysis (EA), thermogravimetric analysis (TG), and powder X-ray diffraction (PXRD). As shown in Figure S1

and Table S1 (Supporting Information), we can find that the as-synthesized samples afford two major weight loss before 320°C, suggesting the chemic formula of $Zn(L)(bpe)\cdot(H_2O)_3(DMF)_{1.5}$. However, immerging in CH_3OH for three days and then degassing under vacuum at 200°C for 24h could not remove the guest DMF molecule completely, and the resulted phase is suggested with the stoichiometry of $Zn(L)(bpe)\cdot(DMF)_{1.2}$ (defined as **ECIT-20@1.2 DMF**). In this regard, but, trying higher temperature degasification will cause collapse of skeleton. Then the activated samples under vacuum at 200°C were used for follow-up investigations of gas adsorption. The diffusion of N_2 at 77K is failed (Figure S3), indicative of poor surface area of the activated samples, mainly due to considerable residual DMF molecules located within this activated material. While, the smaller molecule of CO_2 can diffuse at 195K with the total uptake of 35.6 cm^3/g (1 bar) (Figure 3). The results were consistent with the TG research that the MOF material even after activation still contains considerable guest DMF molecules. And most likely, the occupation of these residues in the MOF channels largely decreases the size of window of channel, especially for the entrance of pore. This can be further reflected in the selective adsorption of CO_2 over CH_4, O_2, CO, and N_2 at 293K (diameter, CO_2‹O_2‹N_2‹ CO_2‹CH_4), where the CO_2 uptake at 1 bar is 6.5 times bigger than that for all other gases (Figure 4).

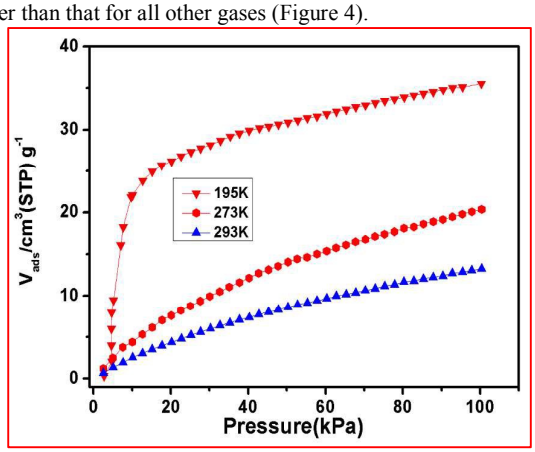

Figure 3. CO_2adsorption isotherms on activated samples at 195K, 273K, and 293K, respectively.

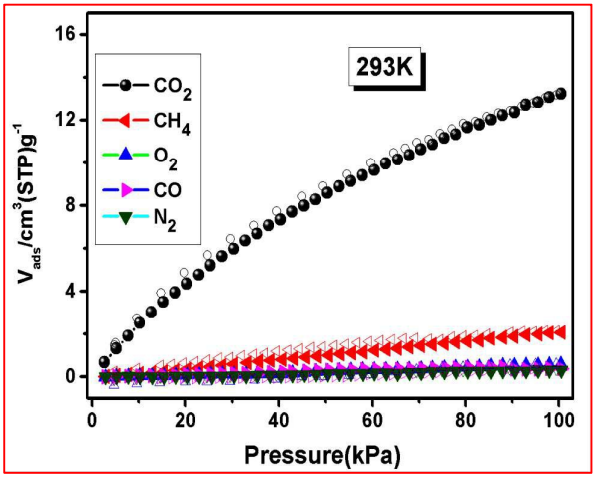

Figure 4. $CO_2/CH_4/O_2/CO/N_2$adsorption isotherms on activated samples at 293K, respectively: adsorption (solid symbols) and desorption (open symbols).

Furthermore, we examined the adsorption of H_2O, CH_3OH, and C_2H_5OH at 298K. The adsorption isotherms were shown in Figure 5, clearly indicative of significant differences among them. Water was slowly adsorbed onto **ECIT-20@1.2DMF** in the low pressure region before P/P_0=0.13, and by contrast, following is a sharp increase as the vapour pressure increased. Finally, the uptake of 63.9 cm^3/g at P/P_0=1 was observed, and desorption segment does not follow the trace of adsorption segment, but giving a big hysteresis. A very similar shaped isotherm was seen for CH_3OH adsorption. However, after the slow adsorption below P/P_0=0.12, the following increase was less sharp, and accompanied was less uptake of 44.4 cm^3/g at P/P_0=0.91. In contrast, C_2H_5OH was adsorbed least with the uptake of 9.2 cm^3/g at P/P_0=0.92. In comparison with above discussed $CO_2/CH_4/O_2/CO/N_2$ adsorption, it is clear that the adsorption of H_2O, CH_3OH should be attributed to typical "gate-opening behavior", just which is dependent on the interaction between MOF adsorbent and adsorbate.[43-47]Correlating this with structure, we found that both the free-standing NO_2- groups and residual DMF molecules in the channels most possibly afford affinity towards H_2O, CH_3OH, and C_2H_5OH, and this most likely caused the occurrence of rotation for NO_2^- groups and/or locomotion of DMF for "gate-opening behavior". But, during this, the size of adsorbate should be also accounted into, like that of C_2H_5OH, where stronger energy to fulfill gate-open adsorption needed for larger size of C_2H_5OH makes the affinity between MOF and adsorbate mismatched.

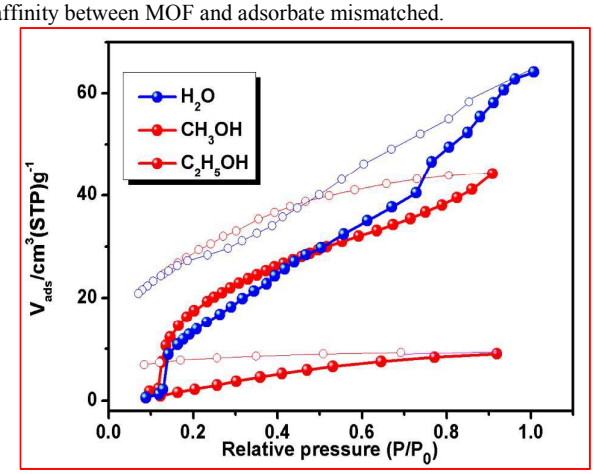

Figure 5. H_2O, CH_3OH, and C_2H_5OH adsorption isotherms on activated samples at 298K, respectively: adsorption (solid symbols) and desorption (open symbols).

Photo-switching Adsorption of Allyl Alcohol. As shown in Figure 6, the activated samples of **ECIT-20@1.2DMF** adsorb allyl alcohol barely, in accordance with the above adsorption rule for H_2O, CH_3OH, and C_2H_5OH, mainly due to the bigger size of allyl alcohol. However, if irradiating under UV at 297nm, this MOF material performs excellent adsorption of allyl alcohol, giving the total uptake of 38.0 cm^3/g, equal to 1.03 mol *per* formula unit. This, combined with large hysteresis between adsorption and desorption isotherms, strongly suggests photo-activated "gate-opening behavior", although without the characteristic 'fingerprint' of step adsorption. If this is true, one critical question, what kind of interaction between MOF and allyl alcohol makes the pore opening, arises. Accordingly, we made an initial assignment of asymmetric [2+2] cycloaddition between bpe C=C bond and allyl alcohol C=C bond. In **ECIT-20** the C=C bonds of bpe ligands located in *b* axis direction aligned parallel but were largely separated by ca. 11.6Å, far beyond the topochemical criteria of less than 4.2 Å,[48-49] thus completely ruled out the possibility of symmetric [2+2] cycloaddition. Similarly, although C=C bonds of other bpe ligands located in *a* axis direction aligned parallel, however, the large separation between them by ca. 11.6Å also prevented the symmetric [2+2] cycloaddition. But, we can anticipate asymmetric [2+2] cycloaddition[50-51]for the C=C bonds

of bpe ligands located in *b* axis direction, rather than that located in *a* axis direction, as where this would be blocked by the tight stacking and C-H…O contacts (ca. 3.7 Å) between HC=CH fragments and L^{2-} NO_2 groups. Correlating the structure with the hypothetical photochemical reaction, the conversion capability is expected to be 0.5mol *per* formula unit for **ECIT-20@1.2DMF**, because steric hindrance would prevent half of bpe ligands to undergo asymmetric [2+2] cycloaddition. Thereby, the total adsorption of 1.03mol *per* formula unit under UV should contain not only the allyl alcohol that occurred asymmetric [2+2] cycloaddition but also additional allyl alcohol that just diffused into the MOF material. This agrees with the final desorption of 0.62 mol *per* formula unit at P/P_0=0.1. To further confirm this, additional CO_2 adsorption experiments were employed as probe to characterize the material after loading allyl alcohol and found that the uptake of the material at full capacity (referenced to 1.03 mol *per* formula unit) or partial filling (referenced to 0.62 mol *per* formula unit) sharply decreased by 73% and 41% (Figure S4). This agrees well with the above discussion that the uptake of allyl alcohol is divided into two parts, one undergoing asymmetric [2+2] cycloaddition and one only diffusing into the MOF material. Furthermore, a series of comparison experiments (see Table 1) were carried out to confirm that this phenomenon was not an experimental or material artefact, but due solely to "gate-opening behavior" in response to photochemical asymmetric [2+2] cycloaddition. Experiments with control materials like that of activated carbon, zeolite, both of which are typical porous materials but without known photoactive unit, and bpe ligand that is a reactant with known photoactive unit but without porosity, showed almost neglectable adsorption variations of allyl alcohol with or without UV irradiation. Accordingly, regardless of whether it is porous but without photoactive unit or nonporous with photoactive unit, similar phenomenon could not be observed in both of them. Especially for bpe ligand, although also with known photoactive unit, however, locating in the porous environment to make it more accessible is crucial. In addition, to exclude the possibility induced by *cis-trans* photoisomerization of bpe ligand inside MOF, the control experiment of CH_3OH and C_2H_5OH adsorption with UV or without UV is undertaken and shown in Figure 7 and S5, indicative of almost no CH_3OH and C_2H_5OH uptake alteration. Furthermore, both single crystal X-ray diffraction and PXRD are used to confirm this, disclosing that both the unit cell and PXRD patterns of **ECIT-20** is not changed even under UV irradiation.

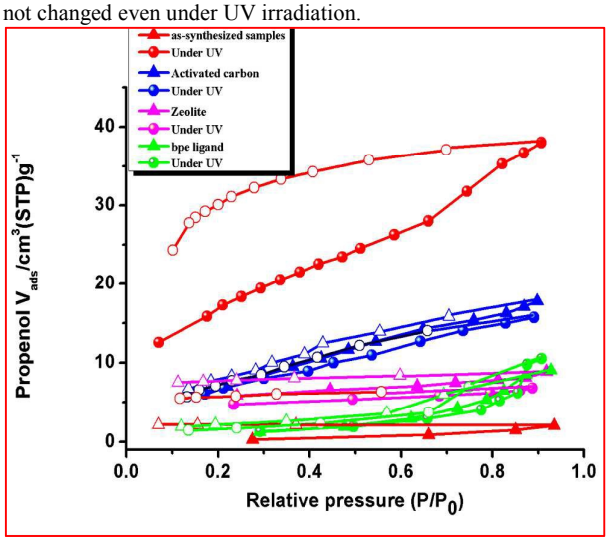

Figure 6. Allyl alcohol adsorption isotherms on **ECIT-20@1.2DMF** and other materials (activated carbon, zeolite, and bpe ligand) at 298K, respectively: adsorption (solid symbols) and desorption (open symbols), without UV (triangle symbols), with UV (round symbols).

Table 1 The comparison of adsorption capability of allyl alcohol under ambience or UV among these control materials.

Materials	Adsorption capability (cm^3/g)	Adsorption capability (cm^3/g) under UV	Alteration
ECIT-20@ 1.2DMF	2.0	38.0	+36 (1800%)
Activated carbon	17.6	15.8	-1.8 (10%)
Zeolite (4A)	8.6	7.0	-1.6 (18%)
bpe ligand	9.0	10.3	+1.3 (14%)

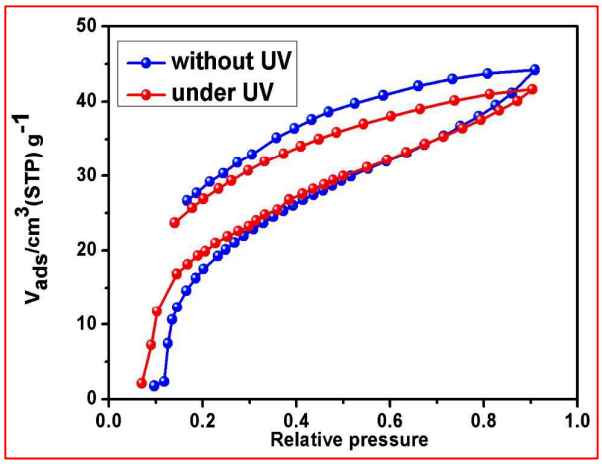

Figure 7. CH_3OH adsorption isotherms on **ECIT-20@1.2DMF** at 298K with UV or without UV, respectively.

To directly disclose this unique asymmetric [2+2] cycloaddition inside **ECIT-20**, single crystal X-ray diffraction would be the best choice. However, unfortunately, the crystal of **ECIT-20** after loading allyl alcohol molecules was destroyed and the structure of the resulted material could not be determined by single crystal X-ray diffraction. But, alternatively, this could be strongly confirmed by TG, infrared spectrum (IR), and ^{1}H MAS plus ^{13}C CPMAS solid-state NMR spectrum. Before taking these tests, we first make an optimal choice of samples, and making a comparison between activated sample and it after finishing an adsorption and desorption circle of allyl alcohol should be one of the best choice, as in this situation allyl alcohol only occurred asymmetric [2+2] cycloaddition inside MOF, rather than diffused inside MOF. As shown in TG plots of Figure S1, the loss of residual DMF molecule advanced before 275°C for activated samples (320°C for fresh samples), and this is further advanced (before 230°C) for the cycloaddition product. Whilst this material underwent the reversible cleavage of cyclobutane rings and then release of allyl alcohol between 230-285°C (exp. 4.3%, calc. 4.2%). This is well consistent with the [2+2] cycloaddition rule that under suitable UV irradiation it occurs, whereas undergoing high temperature will lead it to cleave.[53] In light of this, combined with the EA analysis, we can deduce chemical formula for the cycloaddition product, Zn(L) $(bpe)_{0.5}(bpa)_{0.5}\cdot(DMF)_{1.2}$ (namely **ECIT-21@1.2DMF**, bpa=(2,3-di(pyridin-4-yl) cyclobutyl)methanol). As we know, allyl alcohol is a highly volatile matter and the boiling point of it is around 96°C, suggesting that the loss of it from MOF materials would be facile with the calcinations temperature less than 100°C. By contrast, the above TG results disclosed that the temperature for releasing allyl alcohol from **ECIT-21@1.2DMF** is up to 230-285°C, which strongly implies that the allyl alcohol must undergo certain chemical reaction with MOF skeleton insides **ECIT-20@1.2DMF**, rather than being physically

adsorbed insides **ECIT-20@1.2DMF**. This, coupled with the fact of significant photoswitching behavior towards allyl alcohol inside **ECIT-20@1.2DMF**, and in conjunction with the temperature of releasing allyl alcohol from **ECIT-21@1.2DMF** that is comparable with the value for cleavage of cyclobutane rings observed in the literature,[53] makes us to give the initial assignment, *viz*. asymmetric [2+2] cycloaddition between allyl alcohol and MOF skeleton for this special photoswitching behaviour.

Another evidence for this cycloaddition could be directly reflected by the characteristic IR bond of C=C bond. As shown in Figure 8, IR bond at 958 cm^{-1}, typical of C=C stretching, in **ECIT-21@1.2DMF** decreased sharply, relative to **ECIT-20@1.2DMF**, whilst in **ECIT-21@1.2DMF** the fingerprint bonds for cyclobutane fragment and OH stretching for alcohols were also observed at 2860-2910 cm^{-1} and 3632 cm^{-1}, respectively, thus, strongly suggesting the decrease of C=C bond of bpe ligands and simultaneously formation of cyclobutane.

Further evidences were also obtained by ^{1}H MAS and ^{13}C CPMAS solid-state NMR spectrum in the solid. The samples of **ECIT-20@1.2DMF** only gave one peak around 7.4 ppm covering at 2.3-11.5 ppm, because of the overlapping and broadening of the signals derived from DMF, L and bpe ligands, whereas four additional peaks (3.1 ppm, 3.9 ppm, 4.6 ppm, 6.4 ppm) were observed in **ECIT-21@1.2DMF**.[51] This agree well with the formation of cyclobutane from asymmetric [2+2] cycloaddition between bpe C=C bond and allyl alcohol C=C bond (Figure S6). Further, we can directly observe the alteration of bpe C=C bonds before and after [2+2] cycloaddition in ^{13}C CPMAS solid-state NMR spectrum. As shown in Figure S7, the peak at 129.4 ppm from bpe C=C bond sharply decreased in **ECIT-21@1.2DMF**, because of formation of cyclobutane. Corresponding to this is the appearance of new peak at 62.8 ppm and small humps at 24-59 ppm, suggesting once again the formation of cyclobutane between bpe C=C bond and allyl alcohol C=C bond.[51]

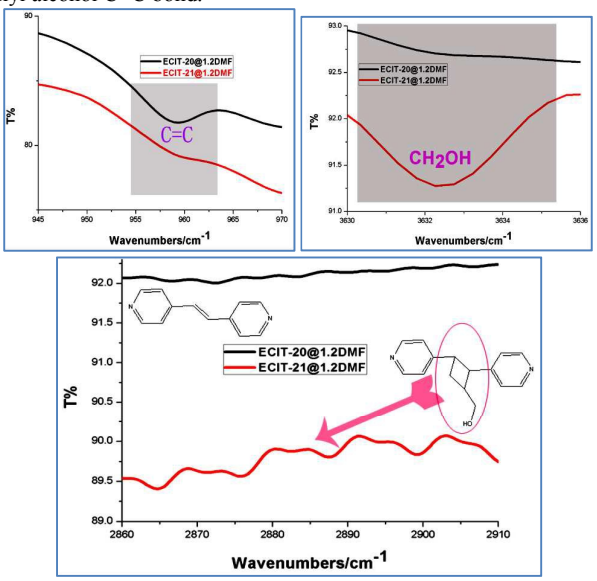

Figure 8. IR spectra of **ECIT-20@1.2DMF** and **ECIT-21@1.2 DMF.**

Furthermore, based on the structure of **ECIT-20@1.2DMF**, the structure of **ECIT-21@1.2DMF** was rationally estimated by DFT calculation (Figure 9). And the simulated PXRD patterns from **ECIT-21@1.2DMF** matched well with that simulated from **ECIT-20@1.2DMF**, suggesting unchanged MOF skeleton even after [2+2] cycloaddition. Moreover, a detailed comparison of experimental PXRD patterns (Figure S2) between **ECIT-20@1.2DMF** and **ECIT-21@1.2DMF** shows that almost all the diffraction peaks of **ECIT-21@1.2DMF** can be exactly indexed to **ECIT-20@1.2 DMF**, except for two sharp peaks observed at approximately 2θ=23.9 and 28.0. This also suggests the same MOF skeleton for **ECIT-21@1.2DMF**. As for the abnormality in PXRD patterns between them, they can be further indexed as (40$\bar{2}$) and (502) in the PXRD patterns as observed in as-synthesized fresh samples, mainly due to the formation of a more dense phase after cycloaddition.

For practical application, the reuse and simple operation is crucial. As shown in Figure 9, based on the above results, the capture/release cycle can be facile to obtain in this way, photochemical [2+2] cycloaddition for capture allyl alcohol and thermo-dependent reversible cleavage of cyclobutane for release of allyl alcohol. Note that the robust MOF material of **ECIT-20@1.2DMF** can maintain the excellent photochemical performance even after four cycles (only decreased by 12%, relative to the first cycle, see Figure S8).

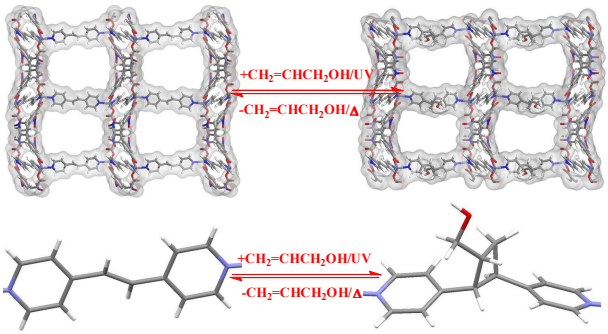

Figure 9. The proposed capture/release cycle for the present MOF material of **ECIT-20** towards high-performance, green, and safe removal and reuse of highly toxic cargo allyl alcohol.

Furthermore, we also concern with the potential applications for the resulted MOF material of **ECIT-21**. As expected, the pore wall of **ECIT-21@1.2DMF** should be fused by extensive, free-standing CH_2OH groups, which arouses us to apply it in removal of Hg^{2+} in aqueous solution.[21-23] Notably, both **ECIT-20@1.2DMF** and **ECIT-21@1.2DMF** performed excellent removal of Hg^{2+} in aqueous solution, but with the adsorption capacity of **ECIT-21@1.2DMF** (230 g/g) exceeding that for **ECIT-20@1.2DMF**(201 g/g) (Figure S11). Improvement also included less time for adsorption equilibrium (100 min for **ECIT-21@1.2DMF** vs. 150 min for **ECIT-20@1.2DMF**) (Figure S9) and higher removal of Hg^{2+} in low concentration (such as 20 ppb: 48.5% for **ECIT-21@1.2DMF** and 34.9% for **ECIT-20@1.2DMF;** 40 ppb: 54.1% for **ECIT-21@1.2DMF** and 43.0% for **ECIT-20@1.2DMF**). Moreover, we also found that such adsorption in **ECIT-21@1.2DMF** is more accordant with the pseudo-second-order kinetic model (Figure S10), relative to that observed in **ECIT-20@1.2DMF**, indicative of more chemical adsorption in **ECIT-21@1.2DMF**.[8d] This agrees well with the predominant, as discussed above, structure in **ECIT-21@1.2 DMF**.

Conclusions

We reported here a novel MOF material, along with its synthesis, structure, adsorption properties, photo-activated chemical reaction, and application in detail. The activated MOF material can exhibit excellent selective CO_2 adsorption over CH_4, N_2, O_2, and CO, and undergo "gate-open behavior", dependent on the strength of host-guest interaction and size of guest molecule. This merit can be further devoted into the

photo-activated gas-solid reaction towards asymmetric [2+2] cycloaddition inside MOF. To some extent, the result has established a distinct PSM method upon photo-activated gas-solid reaction and renovated a pathway to achieve asymmetric [2+2] cycloaddition that could not be facile *via* common method. Our findings of robust MOF showing exceptional photo-switching behavior towards highly toxic allyl alcohol would have practical applications for high-performance, green, and safe removal and reuse of highly toxic allyl alcohol. Most importantly, this discovery launched a distinct and effective approach to facilitate the extensive research on porous MOF materials for capture/release of highly toxic cargo in the near future. Furthermore, the photo-activating gas-solid reaction inside MOF observed here should be also highlighted, as this presents us a renovated method to modify the structure and even function of MOF precursor.

Acknowledgements

This work was supported by the NSF of China (21203022, 21261001, 21361001), the Natural Science Foundation of Jiangxi Province of China (20143ACB20002, 20151BAB203001), and the Young scientist training program of Jiangxi Province of China (no. 20142BCB23018).

Notes and references

1. M. Matsumoto, S. Miura, K. Kikuchi, M. Tamura, K. Masuhiko, K. Hidetaka, Y. Kunio, S. Yamashita, Patent EP 0129802, 1987.
2. Wittcoff, H. A. Reuben, B. G. Plotkin, J. S. *Industrial organic chemicals*, 2nd ed.; John Wiley & Sons, Inc.: Hoboken, New Jersey, 2004.
3. M. Sutter, ED. Silva,N. Duguet, Y. Raoul , E. Métay, M. Lemaire, *Chem. Rev.*, 2015, in press, DOI: 10.1021/cr5004002.
4. R. Matsuda, R. Kitaura, S. Kitagawa, Y. Kubota, R. V. Belosludov, T. C. Kobayashi, H. Sakamoto, T. Chiba, M. Takata, Y. Kawazoe, Y. Mita, *Nature* 2005, **436**, 238..
5. K. Sumida, D. L. Rogow, J. A. Mason, T. M. McDonald, E. D. Bloch, Z. R. Herm, T. Bae, J. R. Long, *Chem. Rev.* 2012, **112**, 724.
6. J. R. Li, J. Sculley, H. C. Zhu, *Chem. Rev.* 2012, **112**, 869.
7. R. B. Getman, Y. S. Bae, C. E. Wilmer, R. Q. Snurr, *Chem. Rev.* 2012, **112**, 703.
8. H. Furukawa, K. E. Cordova, M. O'Keeffe, O. M. Yaghi, *Science* 2013, **341**, 974.
9. J. A. Mason, M. Veenstra, J. R. Long, *Chem. Sci.* 2014, **5**, 32.
10. P. Nugent, Y. Belmabkhout,S. D. Burd,A. J. Cairns,R. Luebke,K. Forrest,T. Pham,S. Q. Ma,B. Space,L. Wojtas,M. Eddaoudi, M. J. Zaworotko, *Nature* 2013, **495**, 80.
11. J. M. Simmons, H. Wu, W. Zhou, T. Yildirim, *Energy Environ. Sci.*, 2011, **4**, 2177.
12. J. A. Mason, K. Sumida, Z. R. Herm, R. Krishna, J. R. Long, *Energy Environ. Sci.* 2011, **4**, 3030.
13. J. M. Huck, L. C. Lin, A. H. Berger, M. N. Shahrak, R. L. Martin, A. S. Bhown, M. Haranczyk, K. Reuter, B. Smit, *Energy Environ. Sci.*, 2014, **7**, 4132.
14. Z. J. Zhang, Z. Z. Yao, S. C. Xiang, B. L. Chen, *Energy Environ. Sci.* 2014, **7**, 2868.
15. Y. B. He, R. Krishna, B. L. Chen, *EnergyEnviron. Sci.* 2012, **5**, 9107.
16. D. Feng, K. Wang, J. Su, T. F. Liu, J. Park, Z. Wei, M. Bosch, A. Yakovenko, X. Zou, H. C. Zhou, *Angew. Chem. Int. Ed.,* 2015, **54**, 149.
17. B. L. Chen, US 8,664,419 B2, 2014.
18. M. Carboni, C. W. Abney, S. B. Liu, W. B. Lin, *Chem. Sci.*, 2013, **4**, 2396.
19. W. T. Yang, Z. Q. Bai,W. Q. Shi,L. Y. Yuan,T. Tian,Z. F. Chai,H. Wang, Z. M. Sun,*Chem. Commun.,* 2013, **49**, 10415.
20. L. L. Wang, F. Luo, L. L. Dang, J. Q. Li, X. L. Wu, S. J. Liu, M. B. Luo, *J. Mater. Chem.A*, 2015, **3**, 13724.
21. K. Yee, N. Reimer, J. Liu, S. Y. Cheng, S. M. Yiu, J. Weber, N. Stock, Z. T. Xu, *J. Am. Chem. Soc.*2013, **135**, 7795.
22. C. W. Abney,J. C. Gilhula, K. Lu, W. Lin, *Adv. Mater.*2014, **47**, 7993.
23. F. Luo, J. L. Chen, L. L. Dang, W. N. Zhou, H. L. Lin, J. Q. Li, S. J. Liu, M. B. Luo, *J. Mater. Chem. A,* 2015, **3**, 9616.
24. S. D. Burd, S. Q. Ma, J. A. Perman, B. J. Sikora, R. Q. Snurr, P. K. Thallapally, J. Tian, L. Wojtas, M. J. Zaworotko, *J. Am. Chem. Soc.* 2012, **134**, 3663.
25. D. S. Li, Y. P. Wu, J. Zhao, J. Zhang, J. Y. Lu, *Coord. Chem. Rev.* 2014, **261**, 1.
26. S. C. Xiang, W. Zhou, J. M. Gallegos, Y. Liu, B. L. Chen, *J. Am. Chem. Soc.*2009, **131**, 12415.
27. T. M. McDonald, J. A. Mason, X. Q. Kong, E. D. Bloch, D. Gygi, A. Dani, V. Crocellá, F. Giordanino, S. O. Odoh, W. S. Drisdell, B. Vlaisavljevich, A. L. Dzubak, R. Poloni, S. K. Schnell, N. Planas, K. Lee, T. Pascal, L. F.Wan, D. Prendergast, J. B. Neaton, B. Smit, J. B. Kortright, L. Gagliardi, S. Bordiga, J. A. Reimer, J. R. Long, *Nature*, 2015, **519**, 303.
28. P. Q. Liao, H. Y. Chen, D. D. Zhou, S. Y. Liu, C. T.He, Z. Rui, H. B. Ji, J. P. Zhang, X. M. Chen, *Energy Environ. Sci.*, 2015, **8**, 1011.
29. P. Q. Liao, A. X. Zhu, W. X. Zhang1, J. P. Zhang, X. M. Chen, *Nat. Commun.* 2015, **6**, 6350.
30. J. Park, D. Q. Yuan, K. T. Pham, J. R. Li, A. Yakovenko, H. C. Zhou, *J. Am. Chem.Soc.*2012, **134**, 99.
31. N. Yanai, T. Uemura, M. Inoue, R. Matsuda, T. Fukushima, M. Tsujimoto, S. Isoda, S. Kitagawa, *J. Am. Chem. Soc.* 2012, **134**, 4501.
32. J. W. Brown, B. L. Henderson, M. D. Kiesz, A. C. Whalley, W. Morris, S. Grunder, H. X. Deng, H. Furukawa, J. I. Zink, J. F. Stoddartc, Omar M. Yaghi, *Chem. Sci.*, 2013, **4**, 2858.
33. R. Lyndon, K. Konstas, B. P. Ladewig, P. D. Southon, C. J. Kepert, M. R. Hill, *Angew. Chem. Int. Ed.* 2013, **52**, 3695.
34. F. Luo, C. B. Fan, M. B. Luo, X. L. Wu, Y. Zhu, S. Z. Pu, W. Y. Xu, G. C. Guo*Angew. Chem. Int. Ed.* 2014, **53**, 9298.
35. D. E. Williams, J. A. Rietman, J. M. Maier, R. Tan, A. B. Greytak, M. D. Smith, J. A. Krause, N. B. Shustova, *J. Am. Chem. Soc.* 2014, **136**, 12201.
36. J. Park, L. B. Sun, Y. P. Chen, Z. Perry, H. C. Zhou, *Angew. Chem. Int. Ed.* 2014, **53**, 5842.
37. D. H. Qu, Q. C. Wang, Q. W. Zhang, X. Ma, H. Tian, *Chem. Rev.* 2015, **115**, 7543.
38. A. J. McConnell, C. S. Wood, P. P. Neelakandan, J. R. Nitschke, *Chem. Rev.* 2015, **115**, 7729.
39. R. D. Mukhopadhyay, V. K. Praveen, A. Ajayaghosh, *Mater. Horiz.*, 2014, **1**, 572.
40. *Materials Studio 7.0*; Accelrys Software Inc., San Diego, CA, 2008.
41. J. P.Perdew, Y. Wang, *Phys. Rev. B* 1986, **33**, 3399.
42. A. L. Spek, *PLATON*, 2001.
43. A. Shigematsu, T. Yamada, H. Kitagawa, *J. Am. Chem. Soc.* 2012, **134**, 13145.
44. H. L. Zhou, Y. B. Zhang, J. P. Zhang, X. M. Chen, *Nat. Commun.*2015, **6**, 6917.
45. S. Takamizawa, *Angew. Chem. Int. Ed.*2015, **54**, 7033.

46. F. Salles, G. Maurin, C. Serre, P. L. Llewellyn, C. Knöfel, H. Jin Choi,Y. Filinchuk, L. Oliviero, A. Vimont, J. R. Long, G. Férey, *J. Am. Chem. Soc.* 2010, **132**, 13782.
47. S. Henke, A. Schneemann, A. Wütscher, R. A. Fischer, *J. Am. Chem. Soc*. 2012, **134**, 9464.
48. D. Liu, Z. G. Ren, H. X. Li, J. P. Lang, N. Y. Li, B. F. Abrahams, *Angew. Chem. Int. Ed.* 2010, **49**, 4767.
49. I. Park, R. Medishetty, H. Lee, C. E. Mulijanto, H. S. Quah, S. S. Lee, J. J. Vittal, *Angew. Chem. Int. Ed.* 2015, **54**, 7313.
50. M. H. Mir, L. L. Koh, G. K. Tan. J. J. Vittal. *Angew.Chem. Int. Ed*. 2010, **49**, 390.
51. M. L. Conner, Y. Xu, M. K. Brown, *J. Am. Chem. Soc.* 2015, **137**, 3482.
52. J. Du, K. L. Skubi, D. M. Schultz, T. P. Yoon, *Science*, 2014, **344**, 392.
53. I. Park, A. Chanthapally, Z. J. Zhang, S. S. Lee, M. J. Zaworotko, J. J. Vittal, *Angew. Chem. Int. Ed.* 2014, **53**, 414.

Removal and safe reuse of highly toxic allyl alcohol by highly selective photo-sensitive metal-organic framework

Feng Luo,[1]* Le Le Gong,[1] Xue Feng Feng,[1] Xian Feng Yi,[2] and An Min Zheng*[2]

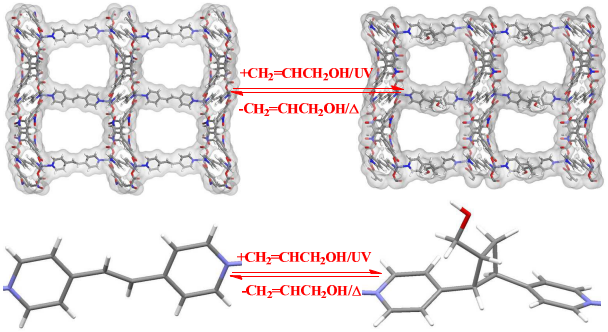

By means of MOF platform and photo-assistant adsorption technique, the green removal and reuse of highly toxic allyl alcohol can be achieved. This is mainly based on a reversible asymmetric [2+2] cycloaddition inside MOF.

Supporting Information

Removal and safe reuse of highly toxic allyl alcohol by highly selective photo-sensitive metal-organic framework

Feng Luo,[1]*Le Le Gong,[1] Xue Feng Feng,[1] Xian Feng Yi,[2] and An Min Zheng*[2]

Table S1. The EA and TG results in this work

Compounds	EA	TG
Zn(L)(bpe)·$(H_2O)_3$$(DMF)_{1.5}$	calc. C/49.41, N/10.38, H/4.42 exp. C/49.23, N/10.31, H/4.36	At 35-320°C, loss all solvents exp. 21.8%, calc. 22.1%
Zn(L)(bpe)·$(DMF)_{1.2}$	calc. C/53.42, N/10.94, H/3.69 exp. C/53.49, N/10.89, H/3.72	At 35-275°C, loss all solvents exp. 13.2%, calc. 13.2%
Zn(L)$(bpa)_{0.5}$$(bpe)_{0.5}$·$(DMF)_{1.2}$	calc. C/53.78, N/10.48, H/3.97 exp. C/53.72, N/10.41, H/3.92	At 35-230°C, loss all solvents exp. 13.2%, calc. 13.2%; At 230-285°C, cleavage of cyclobutane rings and release of allyl alcohol, exp. 4.3%, calc. 4.2%

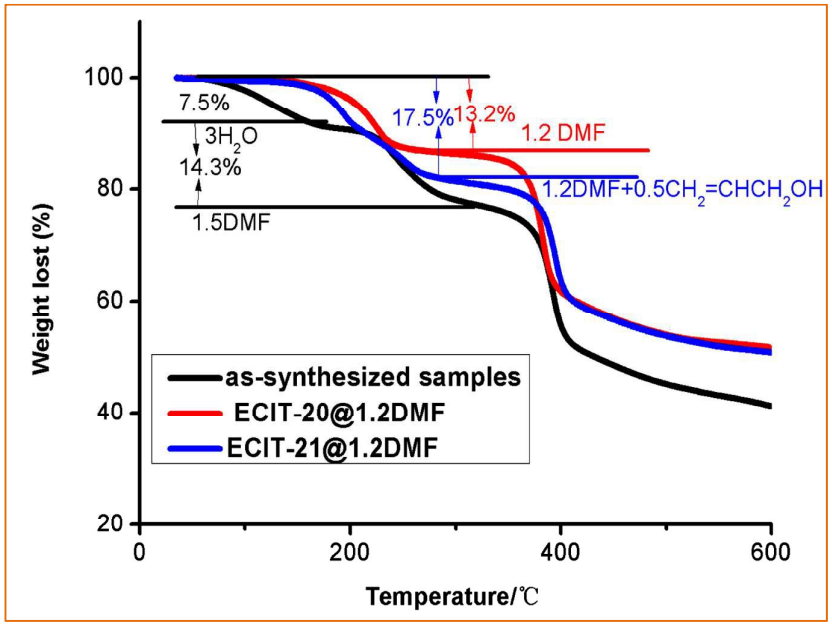

Figure S1. The TG plots in this work.

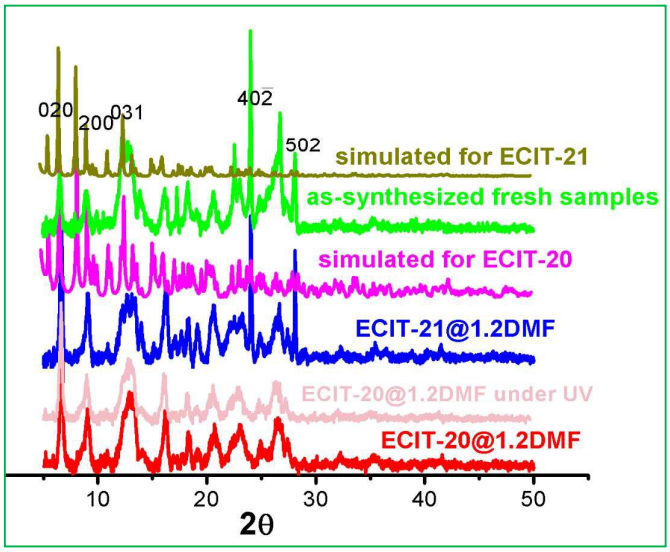

Figure S2. The PXRD patterns in this work.

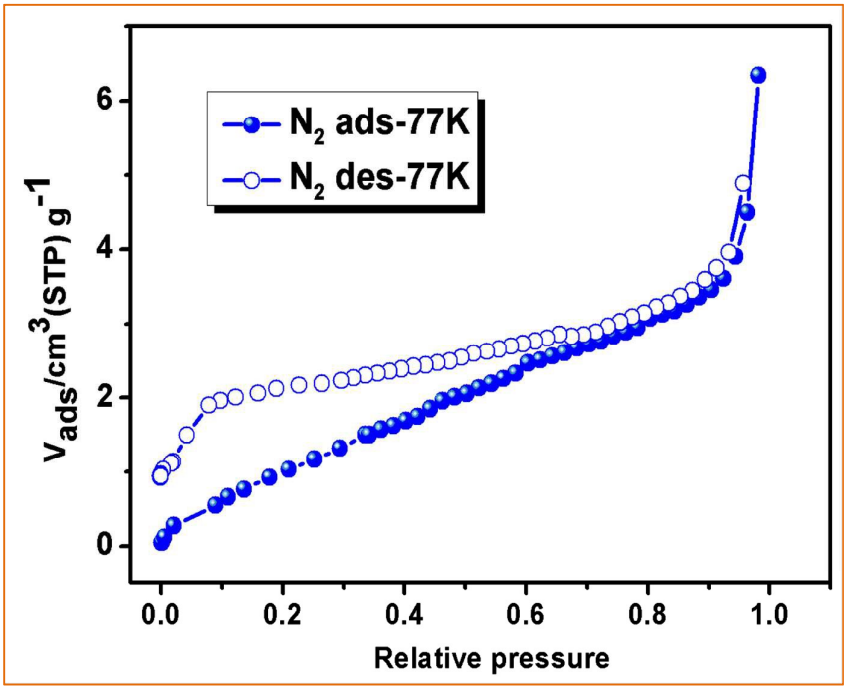

Figure S3. The N_2 adsorption isotherm at 77K for **ECIT-20@1.2DMF**.

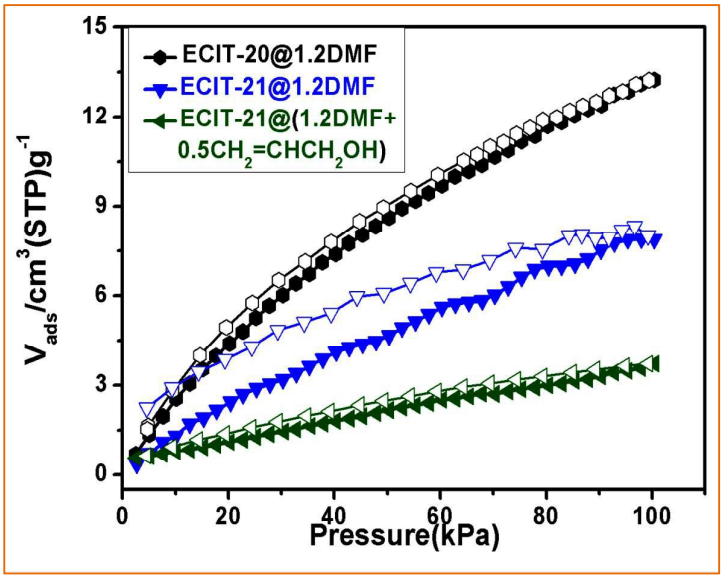

Figure S4. The CO_2 adsorption isotherms at 293 K for **ECIT-20@1.2DMF**, **ECIT-21@1.2DMF**, and **ECIT-21@(1.2DMF+0.5CH_2=$CHCH_2OH$)**, respectively. **ECIT-21@(1.2DMF+0.5CH_2=$CHCH_2OH$)** was obtained in this way that **ECIT-20@1.2DMF** underwent CH_2=$CHCH_2OH$ adsorption under UV but without desorption. Note: adsorption (solid symbols) and desorption (open symbols).

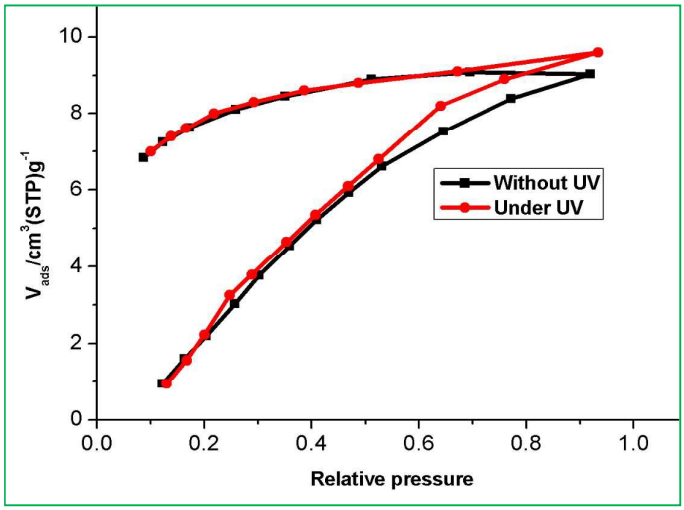

Figure S5. C_2H_5OH adsorption isotherms on **ECIT-20@1.2DMF** at 298K with UV or without UV, respectively.

Solid-State NMR. It was performed at room temperature on a Bruker DRX400-WB instrument. Chemical shifts were referred to external standard adamantane. The broadness would due to chemical shift anisotropy, dipolar and quadrupolar interactions, etc., which was averaged by faster MAS spinning. Due to overlapping and broadening of the signals, complete assignment of chemical

shifts was not attempted.

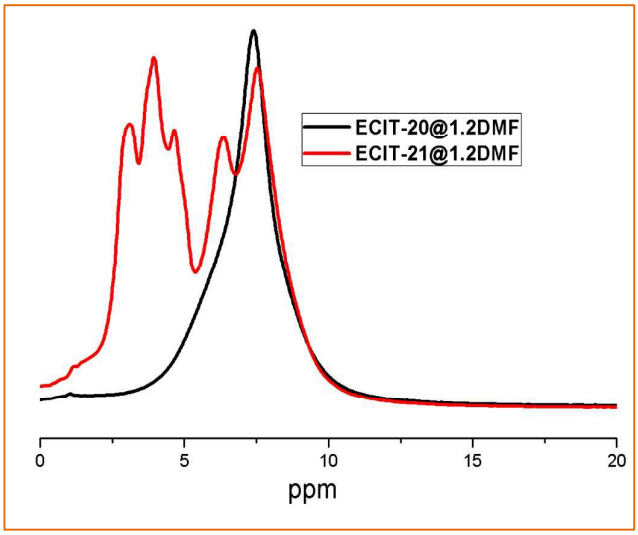

Figure S6. ^{1}H MAS solid-state NMR spectrum of **ECIT-20@1.2DMF** and **ECIT-21@1.2DMF.** The overlapping and broadening of the signals at 2.3-11.5 ppm in **ECIT-20@1.2DMF** is due to DMF, bpe and L ligand. The signals at 3.1 ppm, 3.9 ppm, 4.6 ppm is due to DMF and cyclobutane segment. The signals at 6.4 ppm resulted from partly bpa pyridyl hydrogen atoms close to the cyclobutane segment. The signals at 7.4 ppm resulted from partly bpa pyridyl hydrogen atoms close to the pyridyl nitrogen atom plus L hydrogen atoms.

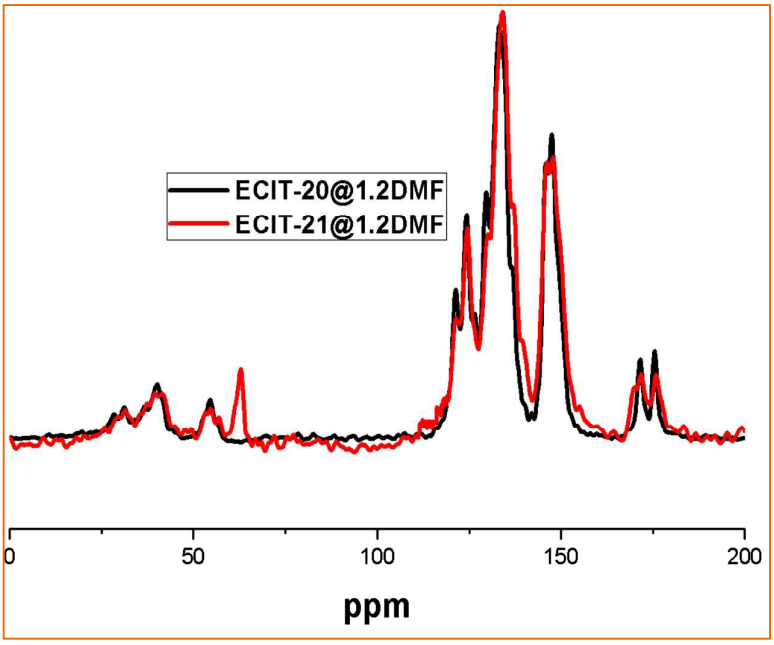

Figure S7. ^{13}C CPMAS solid-state NMR spectrum of **ECIT-20@1.2DMF** and **ECIT-21@1.2DMF.** The signals at 171.2 ppm and 176.2 ppm is derived from DMF C=O fragment and L carboxylate. The peaks at 147.2 ppm, 134.0 ppm, 124.3 ppm 121.3 ppm is due to the bpe, L carbon atoms in

ECIT-20@1.2DMF and bpe, bpa, L carbon atoms in **ECIT-21@1.2DMF**. The peak at 129.4 ppm is assigned to C=C of bpe. Peak at 62.8 ppm should be CH_2OH carbon atoms of cyclobutane segment in **ECIT-21@1.2DMF**. And the small humps at 24-59 ppm is due to DMF and cyclobutane.

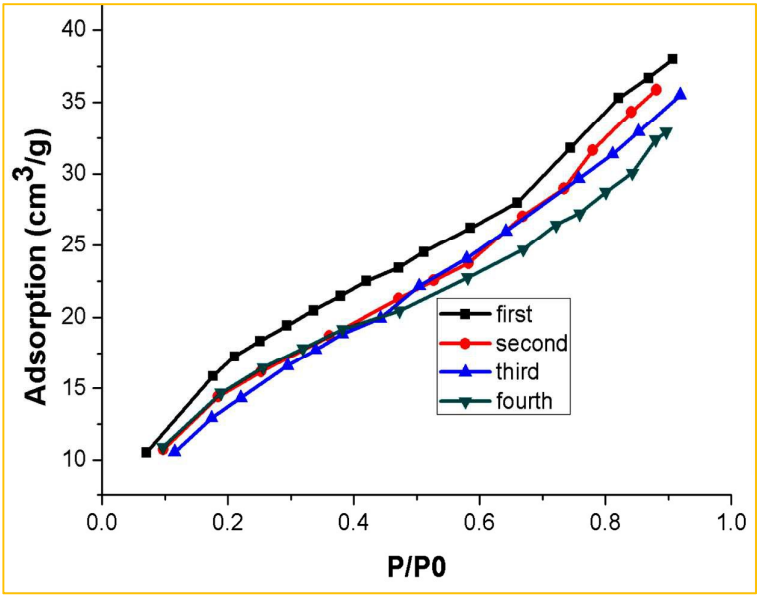

Figure S8. The capture/release cycle obtain in this way, photochemical [2+2] cycloaddition for capture allyl alcohol and thermo-dependent reversible cleavage of cycloaddition for release of allyl alcohol. The samples were prepared in detail as follows: **ECIT-20@1.2DMF** is used to capture allyl alcohol under UV, then the release is by heating the samples after loading allyl alcohol at 285℃ for 24 h.

Hg^{2+} adsorption.A stock solution of Hg(II) (1000 mg L^{-1}) was prepared from $Hg(NO_3)_2$. All the working Hg(II) solutions were prepared using appropriate subsequent dilutions of the stock solution. The adsorption of Hg(II) was carried out under static conditions. The pH of Hg(II) solution was adjusted to the required value by HCl and $NH_3 \cdot H_2O$ solutions. The residual concentration of the Hg^{2+} in the solution was determined by the atomic fuorescence spectrometer (AFS). The amount of adsorption at equilibrium, qe (mg g^{-1}), was calculated according to eqn (1):

$$q_e = \frac{(c_0 - c_e)v}{m} \quad (1)$$

Where c_0 (mg L^{-1}) and c_e(mg L^{-1}) are the initial and equilibrated concentrations of Hg^{2+}, respectively, v (L) is the volume of solution, andm (g) is the mass of dry adsorbent. The removal efficiency (%) of the mercury was calculated by Eq. (2):

$$\text{Removal efficiency (\%)} = \frac{c_0 - c_e}{c_0} \times 100\% \quad (2)$$

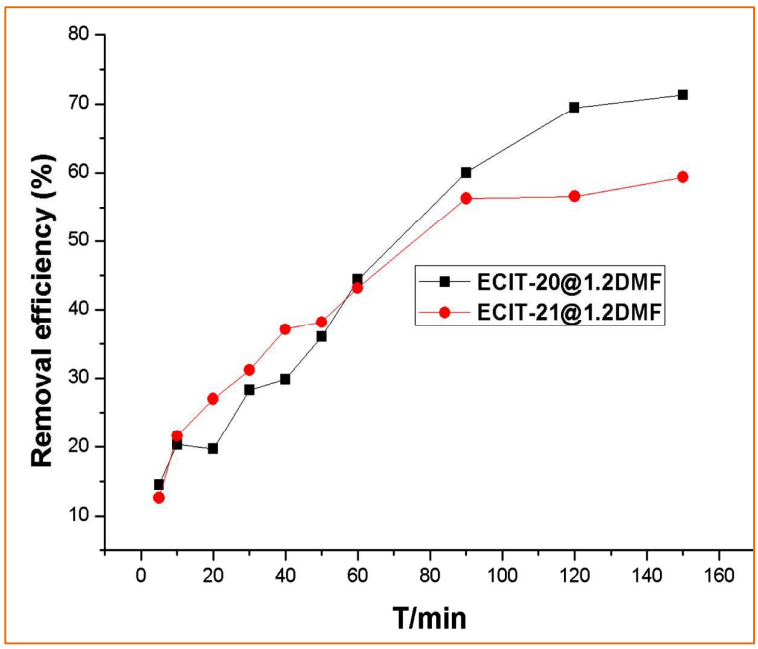

Figure S9. Effect of contact time on Hg^{2+} removal ($c_0(Hg^{2+})$=100 ppb, v=10 mL, m(adsorbent)=2 mg, T=25℃, pH=7).

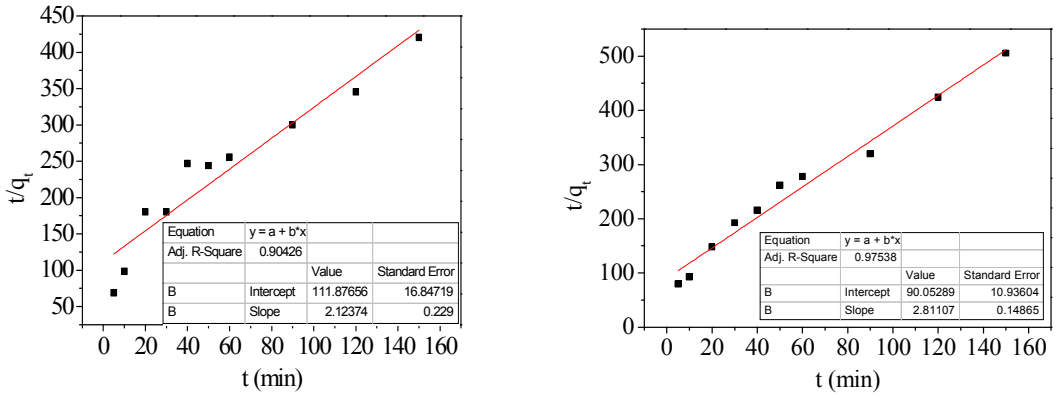

Figure S10. The fitting of pseudo-second-order kinetic plot for the adsorption of Hg^{2+} onto **ECIT-20@1.2DMF**/left and **ECIT-21@1.2DMF**/right, respectively. Note: The pseudo-second-order model is expressed as

$$\frac{t}{q_t} = \frac{1}{k_2 q_e^2} + \frac{t}{q_e}$$

wherek_2 (g (mg min^{-1})) is the pseudo-second-order rate constant, q_e(mg g^{-1}) and q_t (mg g^{-1}) are the adsorption amounts at equilibrium and at time t, respectively. The fitting results were listed as follows: for **ECIT-20@1.2DMF,** k_2=0.04(g/(mg· min)), q_e=0.4709mg/g, $q_{exp.}$=0.3568mg/g; for **ECIT-21@1.2DMF,** k_2=0.0878(g/(mg· min)), q_e=0.3557mg/g, $q_{exp.}$= 0.2967mg/g.

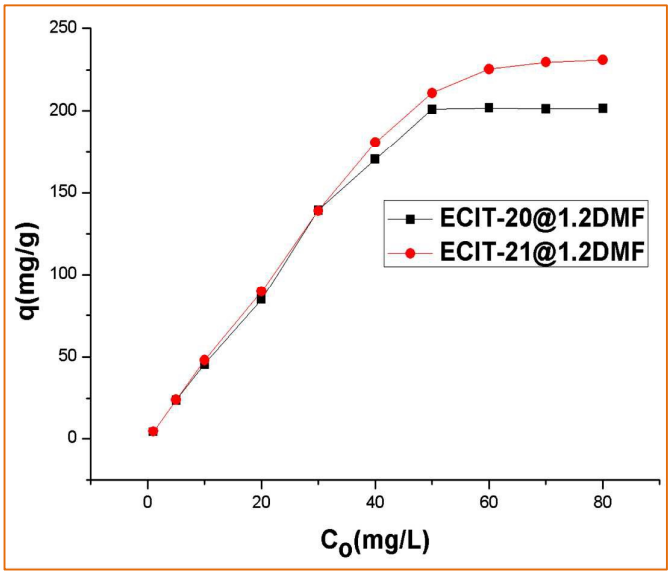

Figure S11. Sorption isotherm of Hg^{2+} for **ECIT-20@1.2DMF** and **ECIT-21@1.2DMF**(v=10 mL, m(adsorbent)=2 mg, T=25℃, t=150 min, pH=7).

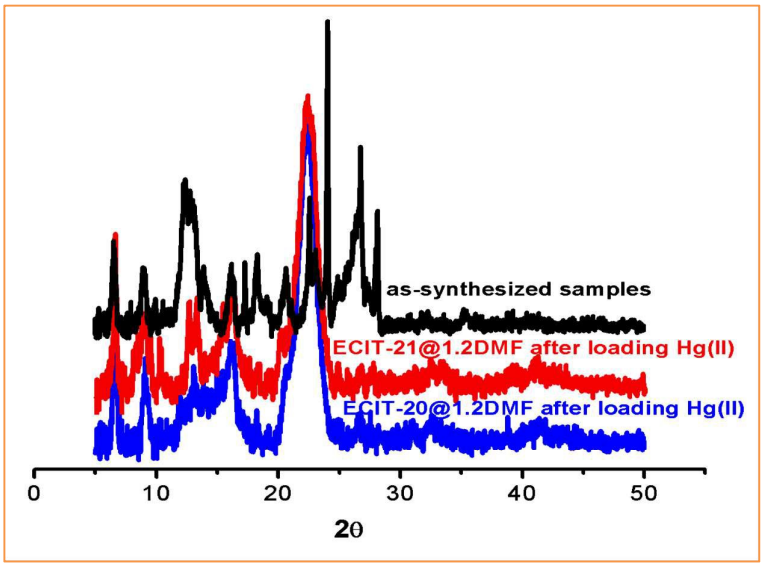

Figure S12. PXRD patterns for the samples of **ECIT-20@1.2DMF** and **ECIT-21@1.2DMF** after loading Hg(II). It is clear that their PXRD patterns match well with the as-synthesized samples, indicating that the skeleton integrity can be maintained even after loading Hg(II). The enhanced and sharp peak at 2θ=22.4 indicates the formation of a more dense phase after loading Hg(II).